Geophysical Research Letters

RESEARCH LETTER
10.1029/2022GL100991

Modulation of the Eastern Equatorial Pacific Seasonal Cycle by Tropical Instability Waves

L. Maillard[1], J. Boucharel[1,2], M. F. Stuecker[3], F.-F. Jin[2], and L. Renault[1]

[1]LEGOS, University of Toulouse, IRD, CNRS, CNES, UPS, Toulouse, France, [2]Department of Atmospheric Sciences, School of Ocean and Earth Science and Technology (SOEST), University of Hawai'i at Mānoa, Honolulu, HI, USA, [3]Department of Oceanography and International Pacific Research Center (IPRC), School of Ocean and Earth Science and Technology (SOEST), University of Hawai'i at Mānoa, Honolulu, HI, USA

Abstract Feedbacks from tropical instability waves (TIWs) on the seasonal cycle of the eastern Pacific Ocean are studied using two eddy-rich ocean simulations, with and without TIWs. By warming the equatorial waters by up to 0.4°C through nonlinear advection in boreal summer and fall, TIWs reduce the amplitude of the seasonal cycle in upper ocean temperatures. In addition, TIWs stabilize the upper part of the Equatorial Undercurrent (EUC) through enhanced barotropic energy conversion, leading to a year-round weakening by -0.15 m s^{-1} and preventing an unrealistic re-intensification in boreal fall usually found in non-eddy resolving models. A coarser simulation at 1-degree horizontal resolution fails to reproduce the TIW-induced nonlinear warming of equatorial waters, but succeeds in inhibiting the EUC re-intensification. This suggests a threshold effect in TIW strength, associated with the model's ability to simulate eddies, which may be responsible for long-standing biases displayed by global climate models in this region.

Plain Language Summary Tropical instability waves (TIWs) are meandering ocean waves that originate off the coast of Ecuador between June and December and propagate in the eastern equatorial Pacific Ocean. By mixing cold equatorial with warm off-equatorial waters, TIWs influence the climate of this key region for the global carbon cycle. In this study, we use a regional ocean model to quantify the impact of these waves on the upper-ocean seasonal cycle. We find that TIWs do not interact in the same way with ocean surface temperatures and currents. TIWs warm surface equatorial waters during the boreal summer and fall, reducing the amplitude of the seasonal temperature cycle. In contrast, TIWs reduce the strength of one of the strongest Pacific equatorial currents—the Equatorial Undercurrent—all year long. Moreover, TIWs prevent an unrealistic re-intensification of this current in boreal fall often found in models unable to simulate these waves accurately. In particular, we provide evidence that the horizontal resolution of most climate models is not sufficient to simulate accurately TIW impacts on the Pacific Ocean, particularly its temperatures. These findings highlight the necessity to incorporate TIW effects in the future generation of global climate models, via enhanced parameterization or increased horizontal resolution.

Key Points:

- Feedbacks from tropical instability waves (TIWs) on the eastern equatorial Pacific Ocean seasonal cycle are quantified
- TIWs reduce the amplitude of the upper equatorial ocean temperature seasonal cycle by warming equatorial waters in boreal summer and fall
- TIWs stabilize and weaken the upper Equatorial Undercurrent year-round and prevent its re-intensification in boreal fall

Supporting Information:

Supporting Information may be found in the online version of this article.

Correspondence to:

L. Maillard,
lisa.maillard@univ-tlse3.fr

Citation:

Maillard, L., Boucharel, J., Stuecker, M. F., Jin, F.-F., & Renault, L. (2022). Modulation of the eastern equatorial Pacific seasonal cycle by tropical instability waves. *Geophysical Research Letters*, *49*, e2022GL100991. https://doi.org/10.1029/2022GL100991

Received 24 AUG 2022
Accepted 10 NOV 2022

1. Introduction

Tropical instability waves (TIWs) are long waves with wavelength of 800–2,000 km and period of 15–40 days (Lyman et al., 2007; Qiao & Weisberg, 1995), that propagate westward at the surface of the equatorial Pacific Ocean. They are observed through meanders of surface tracers such as temperature, salinity and oxygen (Lee et al., 2012; Legeckis, 1977), and alternating cusps of meridional velocities (Düing et al., 1975; Qiao & Weisberg, 1995), sea surface height (Escobar-Franco et al., 2022; Miller et al., 1985), and winds (Chelton et al., 2001; Xie et al., 1998).

TIWs represent the dominant form of oceanic mesoscale activity in the tropics. They are generated by baroclinic and barotropic conversions of energy that are respectively related to the mean meridional gradient of temperature between the cold equatorial upwelled water and the surrounding warm tropical waters (Cox, 1980; Masina et al., 1999; Z. Yu et al., 1995), and to the meridional shear of zonal equatorial currents (Philander, 1976, 1978).

TIWs modulate the climate variability of the tropical Pacific through complex two-way interactions over a wide range of timescales, from intraseasonal to interannual. For instance, TIWs warm the cold tongue and reduce the meridional gradient of temperature in a direct way, mostly via meridional Nonlinear Dynamical Heating (NDH, i.e., advection of anomalous temperatures by anomalous currents. See Graham, 2014; Im et al., 2012; Menkes

et al., 2006). They also reduce the average strength of equatorial currents and in particular the EUC. This reduces the volume of warm subsurface water brought from the western Pacific into the cold tongue, leading to a rectified cooling effect that partly counterbalances the direct TIW warming through NDH (Maillard et al., 2022). By modulating the heat and momentum budgets, TIWs have a complex impact on the mean flow of active and passive tracers, which together with their strong effect on the vertical oceanic mixing (Holmes & Thomas, 2015; Inoue et al., 2012; Lien et al., 2008; Moum et al., 2009) can substantially influence biogeochemical properties (Eddebbar et al., 2021) in this key region for ecosystems and the global carbon cycle (Takahashi et al., 2009).

TIWs are also at the heart of another well-known nonlinear interaction between intraseasonal timescales and the El Niño-Southern Oscillation (ENSO), the strongest driver of interannual variability in this region. ENSO modulates TIW activity, enhancing it during La Niña and decreasing it during El Niño (An, 2008; Wang & McPhaden, 2000, 2001). In turn, TIWs warm the cold tongue more during La Niña than El Niño, leading to an asymmetric negative feedback that may partially explain the observed asymmetry in ENSO amplitude (e.g., An, 2008; An & Jin, 2004; Vialard et al., 2001). More recently, Boucharel and Jin (2020) developed an analytical formulation of the amplitude of TIWs that is modulated by both ENSO and the seasonal cycle. This formulation successfully reproduces the feedback of TIWs on ENSO, through the seasonal modulation of the NDH generated by TIWs (Xue et al., 2020, 2021). These studies highlight the central role played by the seasonal cycle in these multi-scale interactions between ENSO, TIWs, and the climate background state.

Despite a roughly constant equatorial solar shortwave heat flux, the equatorial sea surface temperature (SST) and zonal currents have a pronounced seasonal cycle. TIWs are therefore modulated at seasonal timescales (Im et al., 2012; Von Schuckmann et al., 2008; M. Wang et al., 2019). The intensification of trade winds above the cold tongue region during the second half of the calendar year increases the equatorial upwelling and meridional temperature gradient and strengthens the South Equatorial Current, enhancing TIW activity from July to February (e.g., Contreras, 2002). However, the feedback of TIWs onto the eastern Pacific seasonal cycle has received much less attention since the seminal study by Im et al. (2012). Using an eddy-permitting ocean model, they suggested that the intensified TIW activity in boreal summer and fall warms the eastern equatorial Pacific SST due to in-phase NDH, by up to 1°C month^{-1} during the active TIW period. This feedback between seasonal and intraseasonal variability requires a more in-depth study to fully understand the complex multi-scale interactions at the heart of which TIWs are embedded.

In this study, we build up on the methodology developed and validated in Maillard et al. (2022) to evaluate and quantify TIW effects on the seasonal variations of the eastern equatorial Pacific thermo-dynamical properties. More specifically, we compare twin long-term regional 1/12° ocean simulations in which TIWs freely develop (TIW-RUN) or are removed (NOTIW-RUN). This technique allows us to explicitly quantify the rectified effects of TIWs on the seasonal cycle of the main thermal and dynamical features. We also compare two additional coarser resolution simulations (1° horizontal resolution), with (LR-RUN) and without non-linear terms in the momentum equation (NONL-RUN) to investigate to which extent low-resolution simulations with distinctly degraded TIW activity can reproduce the TIW-induced modulation of the eastern Pacific seasonal cycle. In the first result section, we show that the control TIW-RUN reproduces well the main characteristics of the observed TIW seasonal cycle. In Section 2, we focus on the impact of TIWs on the seasonal cycle of thermal and thermo-dynamical features of the upper ocean. The third section details the impact of TIWs on the seasonal cycle of dynamical features, with a particular emphasis on the EUC. The last section summarizes and discusses our results.

2. Model and Methods

The numerical model and configurations are the ones employed in Maillard et al. (2022), and the following model descriptions are derived from it with minor modifications. The reader is invited to refer to that study for more details.

Ocean model simulations were performed using the coastal and regional ocean community model (CROCO, Debreu et al., 2012; Shchepetkin, 2015; Shchepetkin & McWilliams, 2005, 2009). CROCO is a free-surface, terrain-following coordinate model with split-explicit time stepping and with Boussinesq and hydrostatic approximations. CROCO is implemented over the eastern tropical Pacific ocean (20°S–40°N, 185°–68°W). Tracers, surface elevation, and horizontal velocity initial and boundary information are derived from the Simple Ocean Data Assimilation 5-day reanalysis (SODA v3.4.2 on a 1/4° × 1/4° horizontal grid, Carton et al., 2018). The

bathymetry is obtained from the Shuttle Radar Topography Mission (SRTM30 plus, Becker et al., 2009). The terrain-following configuration has 50 vertical σ-levels, with stretching surface and bottom parameters of $\theta_s = 7$, $\theta_b = 2$, and $h_{\text{cline}} = 200$ m. The K-profile parameterization is used to compute the vertical mixing of tracers and momentum (KPP; Large et al., 1994). The surface freshwater, heat, and momentum fluxes are estimated using the Coupled Ocean-Atmosphere Response Experiment bulk formulas (Fairall et al., 2003) with a surface stress-correction approach described in Renault et al. (2016, 2020). The precipitation rate, the wind field at 10-m, the shortwave and longwave radiation flux, and the temperature and specific humidity at 2-m are derived from the hourly Climate Forecast System Reanalysis (CFSR and CFSv2, Saha et al., 2010, 2011).

Four simulations are performed after a spin up of 7 years, and each four configurations is detailed hereafter and in Table S1 in Supporting Information S1. A set of two eddy-rich ($dx = 1/12°$) simulations is carried out:

- TIW-RUN, in which TIWs are free to develop and propagate;
- NOTIW-RUN, in which TIWs are damped. One more year of spin up is done for this simulation to ensure its stabilization.

Following Maillard et al. (2022), in NOTIW-RUN, to damp TIWs, the meridional currents v in the region of active TIWs are nudged online toward their monthly climatology calculated from TIW-RUN. This methodology removes most of TIW activity while keeping the equatorial dynamics and in particular the Kelvin wave activity mostly untouched. Indeed, only the amplitude of Kelvin waves is slightly different between TIW- and NOTIW-RUN (see Maillard et al. (2022), their Figures 7c and 7d), which might be due to the TIW-Kelvin wave interactions (Escobar-Franco et al., 2022; Holmes & Thomas, 2016) or to the TIW-induced modification of the mean state. These two eddy-rich simulations are used to isolate the effect of TIWs on the ocean mean state, by subtracting the NOTIW-RUN from the TIW-RUN. Another set of two coarse-resolution ($dx = 1°$) simulations is performed:

- LR-RUN is used to test the ability of a model with similar horizontal resolution as most climate models used in the Coupled Model Intercomparison Project Phase 6 (CMIP6, Eyring et al., 2016) to reproduce TIW-induced modulations of the eastern equatorial Pacific seasonal cycle.
- NONL-RUN, in which non-linear terms in the momentum balance equation are disabled (see Gruber et al., 2011) largely reducing TIW activity through a less subtle technique.

3. Results

3.1. TIW Seasonality in the Ocean Model

To evaluate the ability of the TIW-RUN to reproduce TIW variability, we compare simulated and observed variances of intraseasonal anomalies of SST (SST'^2) and meridional surface currents (v'^2), based on 30-day high-pass filtered data. Next, a spatial high-pass filter of 12° longitude is applied to isolate fine-scale structures associated with TIWs. Note that a 5-day low-pass filter is also applied to observations to remove high frequency variability. Spatial and temporal filtering are performed by applying a centered running mean to the data.

Figures 1a and 1b show the long-term mean of SST'^2 from the TIW-RUN and the observations (daily NOAA 1/4° Optimal Interpolation SST OISST v2 from January 1981 to December 2019, Reynolds et al., 2007). The spatial patterns of SST'^2 are very similar, yet with an amplitude slightly overestimated in TIW-RUN compared to observations (+26% in the black box, 2°–5°N, 160°–110°W). The seasonal cycle of the simulated SST'^2 has the same phase and displays a similar amplitude as the observations (Figure 1e), and the monthly time-series of the simulated SST'^2 closely follows the observed interannual variations (Figure 1g) with a Pearson correlation coefficient of 0.85 (99% confidence level, see Text S1 in Supporting Information S1).

Figures 1c and 1d show the long-term mean of v'^2 from the TIW-RUN and the observations (daily altimetric geostrophic and modeled Ekman currents from the GlobCurrent project at 1/4° from January 1993 to May 2017, Rio et al., 2014). The model reproduces well the observed dipole structure, yet with a stronger near-equatorial peak. However, the GlobCurrent currents might not be accurate at the equator, and several reanalyses (e.g., GLORYS12, HYCOM, ECCO2 and GODAS) show contrasted patterns and intensities of v'^2 (Xue et al., 2022). Nevertheless, the v'^2 pattern in TIW-RUN is consistent with most reanalyses products, and with the standard deviation pattern of v' obtained from altimeters in M. Wang et al. (2020). The box-averaged seasonality of v'^2

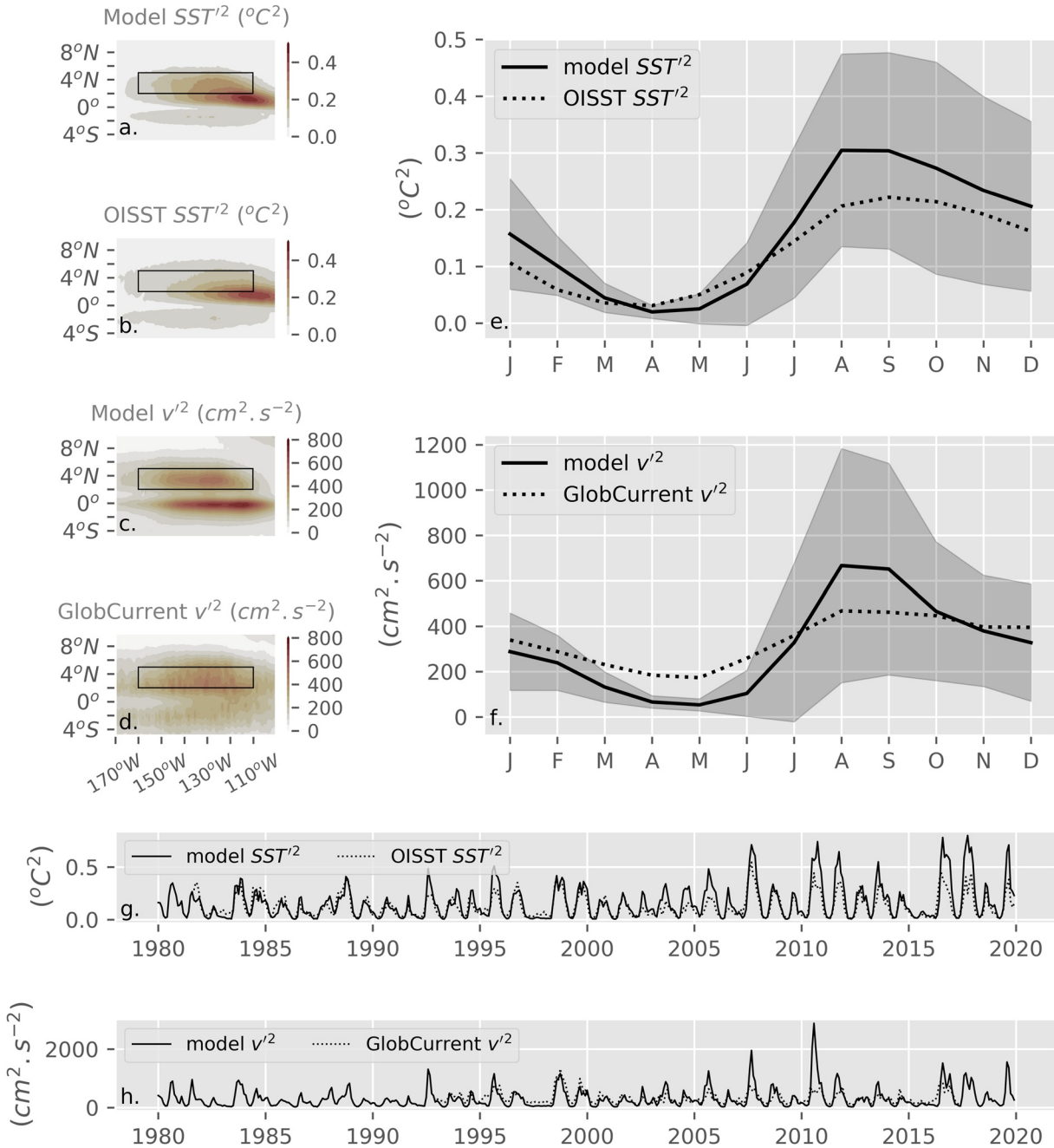

Figure 1. Maps of mean tropical instability wave (TIW) variance SST′² in (a) the simulated TIW-RUN (1980–2019), and (b) observed OISST (1981–2019), (c, d) Same as (a, b) but for the TIW variance v'^2, in (c) the simulated TIW-RUN (1980–2019) and (d) GlobCurrent product (1993–2017). (e) Annual cycle of SST′² averaged over the region 2°–5°N, 160°–110°W (black box in (a–d)). Shading shows the interannual variability of the model (±1 std). (f) Same as (e) for v'^2. (g) Monthly time series of SST′² averaged over the same region. (h) Same as (g) for v'^2.

follows that of SST′² (Figure 1f), and confirms that TIWs are active from July to February, in good agreement with the observations.

The interannual variability of TIW variance is shown in shading in Figures 1e and 1f, and by the monthly time-series of v'^2 and SST′² in Figures 1g and 1h. The intensity of TIW variance greatly varies from one year to another. For instance, the 2015 El Niño period leads to an almost nonexistent TIW activity whereas the TIW signal is very strong during the following La Niña events of 2016 and 2017. Boucharel and Jin (2020) demonstrated in their Figure 3c that most of this interannual variability is dominated by ENSO, and by the amplitude

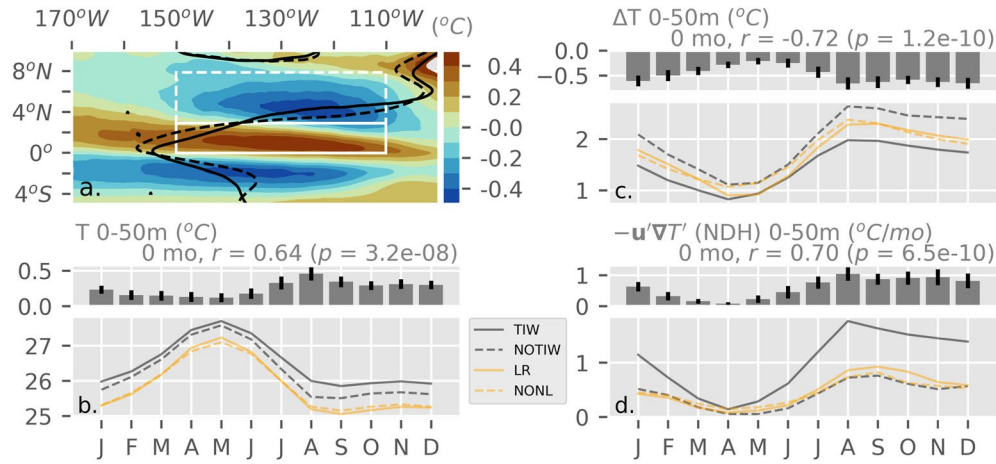

Figure 2. Impact of tropical instability waves (TIW) on the upper temperature seasonal cycle. (a) Map of the 50-m averaged temperature difference between TIW- and NOTIW-RUN (colors). The 27.5°C isotherm is shown in plain and dashed bold contours for TIW- and NOTIW-RUN respectively. (b) Seasonal cycle of TIW-RUN (solid gray line), NOTIW-RUN (dashed gray), LR-RUN (solid orange), and NONL-RUN (dashed orange), and difference between TIW- and NOTIW-RUN (gray bars) for the mean temperature averaged over the first 50 m in the plain-line white box (0°–3°N, 150°–110°W). (c) Same as (b) but for the meridional temperature difference between dashed-line white box (3°–8°N, 150°–110°W) and plain-line white box averages. (d) Same as (b) but for NDH averaged in the plain-line white box. Error bars denote the interannual variability (set to ±0.5 std for clarity). The lag (e.g., "2 mo," in month), the Pearson correlation coefficient r and its p-value are obtained from a lead-lag analysis between the TIW index and the difference between TIW- and NOTIW-RUN for the variable of interest.

modulation emerging from the nonlinear interaction between ENSO and the annual cycle, the so-called combination mode (Stuecker et al., 2013).

Overall, the simulation captures well the TIW seasonal and interannual variability. In the following, a "TIW index" is defined as the monthly average of v'^2, averaged over the black box in Figure 1. Similar results are obtained when using SST'^2 as the TIW index (Table S2 in Supporting Information S1). The same diagnostic is performed on NOTIW-, LR-, and NONL-RUN and compared to the TIW-RUN (Figure S1 in Supporting Information S1). In the NOTIW-RUN most of TIW variability is removed (removal of 91% of v'^2 and 70% of SST'^2). The LR-RUN still reproduces half of TIW variability. In NONL-RUN, only SST'^2 is used to characterize TIW variability since this method creates a spurious noise in the velocities (Gruber et al., 2011). This last experiment simulates only 19% of SST'^2.

3.2. TIW Influence on the Upper-Ocean Temperature Seasonal Cycle

Cold upwelled waters near the equator (Figure 2a, averaged in the region delineated by white solid-lines, and from 0 to 50 m) are subject to a strong annual cycle, being warmer from March to June and colder from August to January (Figure 2b, curves). These cold waters are situated next to warm tropical waters, creating a similarly phased meridional gradient of temperature. Here, we use the 50-m averaged temperature difference between the northern off-equatorial (averaged in the region delineated by white dashed-lines) and equatorial (averaged in the region delineated by white solid-lines) waters as a proxy of the meridional temperature gradient (Figure 2c). This strong gradient participates in the generation of TIWs through baroclinic instability, which in turn warms the cold upwelled waters via NDH during the period of active TIWs (Figure 2d, solid gray line). Here, the NDH is defined as the 3-dimensional TIW nonlinear advection of heat $-\boldsymbol{u}'\nabla\boldsymbol{T}'$ over the first 50 m, with primes denoting fluctuations from a temporal 30-day running-mean. On average, TIWs warm waters between 0° and 3°N by up to 0.4°C in the first 50 m and cool the northern tropical waters by the same amount, decreasing the northward meridional temperature gradient (see Figures 2a and 2c and Maillard et al., 2022). This process expands the cold tongue in the meridional direction, as depicted by the 27.5°C isotherms of TIW-RUN (solid black line) and NOTIW-RUN (dashed black line), with their meridional extent differing by 100 km at 140°W.

In order to quantify TIW seasonal impacts on these thermal features, the differences in the annual cycles between TIW- and NOTIW-RUN are indicated in gray bars in Figures 2b–2d. We also performed a lead-lag correlation analysis between the TIW-induced differences and the TIW index, to evaluate a potential delayed impact of TIWs on the thermal features. This lead-lag correlation analysis is simply giving the delay for which the two signals have the highest Pearson correlation coefficient. The impact of TIWs on upper ocean temperature, meridional temperature gradient, and NDH is shown to be highly correlated with TIW activity, with correlation coefficients of 0.64, −0.72, and 0.70 respectively (99% confidence level) and null lag values indicating a strong and sub-monthly amplitude modulation of the upper thermal oceanic structure by TIW-induced NDH, consistent with the study of Im et al. (2012). In particular, the impact of TIWs on thermal characteristics is stronger in boreal summer and fall (and stays significant until mid-winter, in particular for the meridional temperature gradient), when equatorial surface ocean temperatures are the coldest and the meridional temperature gradient is the strongest, than in boreal spring when the situation is reversed (Figures 2b and 2c). This leads to a reduction of the amplitudes of both equatorial surface ocean temperatures and meridional gradient seasonal cycles.

We emphasize that while the NDH is not increased by TIWs during the non-active TIW season (Figure 2d, bars in March-April are not significantly different from zero), we still notice a slight increase of the temperature (0.2 ± 0.1°C in March) and a moderate decrease (-0.4 ± 0.2°C in March) of the meridional temperature gradient in this season. Therefore, TIWs are inducing a change in the seasonal cycle, which is not restricted to the period of active TIWs. This could indicate a more long-term impact of TIWs on the mean thermal state, with an integration over time of the fluctuating changes induced by TIWs.

Compared to the TIW-RUN, the LR-RUN (solid orange line) underestimates NDH, most likely due to its reduced TIW activity described in Section 3.1. Such low NDH can explain the overestimated meridional temperature gradient, and the underestimated equatorial temperature. However, the cold tongue temperature in the LR-RUN is 0.4°C cooler on average than in the NOTIW-RUN, despite similar amplitude of the NDH. This suggests that reducing the horizontal resolution not only impacts TIW activity but also other circulation and dynamical features, making it difficult to disentangle the changes induced by TIWs from other changes associated with the decrease in resolution in this simulation. Compared to the LR-RUN, the NONL-RUN (dashed orange line) displays slightly weaker NDH from April to November due to weaker TIW activity, and an increased meridional temperature gradient from April to August, that is, the less active TIW period. This is counter-intuitive, as we would expect the difference to be strongest during the active TIW period. This suggests that other processes involving nonlinear momentum terms are modifying the large scale environment. Overall, the NONL-RUN is very similar to the LR-RUN, indicating no improvement in the ability of the LR-RUN to capture the TIW-induced NDH warming of equatorial waters.

3.3. TIW Influence on the Equatorial Undercurrent Seasonal Cycle

The EUC plays an essential role in the Pacific Ocean, transporting large amounts of water to the east along the equatorial thermocline. The EUC evolves zonally, getting closer to the surface as it flows eastward especially from April to May, when trade winds are weak (X. Yu & McPhaden, 1999). Here we evaluate its properties over the region where TIWs are the most active (140° − 120°W), that is, where they most likely are able to induce large-scale circulation changes. The seasonal cycles of the EUC peak value and of the EUC transport are shown in Figures 3a and 3b. The impact of TIWs on the peak value of the EUC and on its transport is illustrated by the gray bars.

The first remarkable result is the year-long TIW-induced reduction of the EUC strength of -0.15 ± 0.02 m s^{-1} on average (Figure 3a), highlighting a time-integrated effect of TIW activity onto the EUC annual cycle. This is confirmed by the one-to-two months lags and moderate values of correlation coefficients with TIW activity (2-, 1-month lags and −0.38, −0.54 correlation coefficients, with 85% and 99% confidence levels respectively for the peak value and transport).

To investigate the dynamical processes at play behind this seasonal rectification of the EUC, Figures 3c and 3d shows the climatology of $\left(1 - \partial_y^2 u/\beta\right)$ (shading) and of the dominant term of the barotropic conversion rate (thin contours) defined as $-u'v'\partial_y u$ with primes denoting deviations from a temporal 30-day running mean only. According to the Rayleigh-Kuo's inflection theorem (lanKuo, 1949), a necessary condition for a flow to be barotropically unstable is that the gradient of the absolute vorticity, $\beta - \partial_y^2 u$, changes sign and thus somewhere

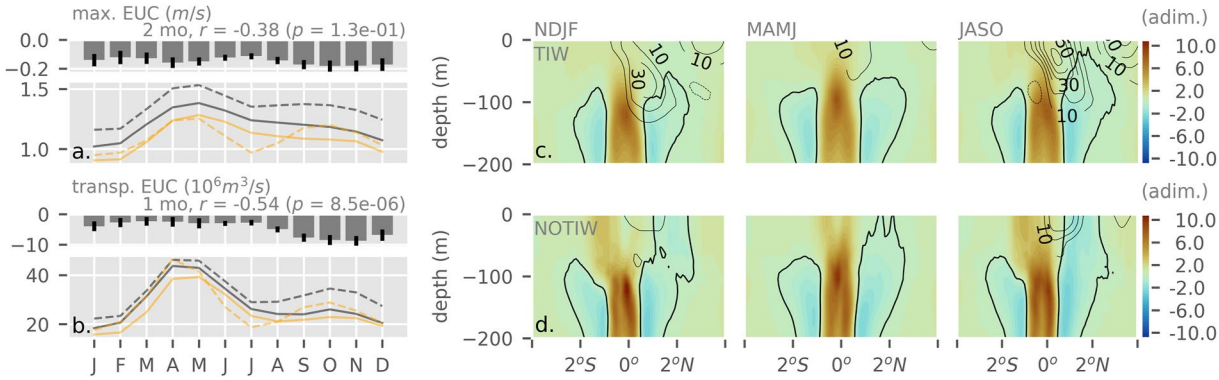

Figure 3. Impact of tropical instability waves (TIW) on the Equatorial Undercurrent (EUC) seasonal cycle. (a) Seasonal cycle of TIW-RUN (solid gray line), NOTIW-RUN (dashed gray), LR-RUN (solid orange) and NONL-RUN (dashed orange), and difference between TIW- and NOTIW-RUN (gray bars) for the maximum value of EUC (maximum of the eastward u averaged between 140°–120°W, in the 4°S–3°N and 0–200 m range). (b) Same as (a) but for the mean value of the EUC transport (eastward u integrated between 4°S–3°N, 140°–120°W, 0–200 m). (c) Depth-latitude sections of the barotropic instability criterion (shading) and barotropic conversion rate (thin contours every 10×10^{-5} cm^2 s^{-2}) for TIW-RUN for each climatological season (November to February (left), March to June (middle) and July to October (right)), averaged between 140°–120°W. (d) Same as (c) but for the NOTIW-RUN. Bold contours depict the zero value of the instability criterion, that is, the locations satisfying the Rayleigh criterion of barotropic instability.

$\left(1 - \partial_y^2 u/\beta\right) = 0$. Areas where this criterion is satisfied are shown in black bold contours for TIW-RUN (Figure 3c) and NOTIW-RUN (Figure 3d). In both runs, this criterion is satisfied between 100–200 m depth on each side of the equator. In the NOTIW-RUN, the criterion is also met in the upper 100 m in the Northern Hemisphere, all year long (see also Figure S2 in Supporting Information S1) while it is most of the time maintained below 50–100 m depth in the TIW-RUN. This potential stabilization of the upper layer could occur through the barotropic conversion of energy, as indicated by the thin contours in Figure 3c. This conversion is responsible for the formation of TIWs, which highlights their key role in stabilizing the near surface ocean. By contrast, TIWs in the NOTIW-RUN are too weak to break this unstable state by converting the mean energy contained in the EUC into eddy energy. The unstable state therefore persists all year, concurrently with the observed permanent stronger EUC in the absence of TIWs.

The second intriguing result is the near disappearance of the second seasonal maximum in EUC intensity and transport during the second half of the calendar year, in the TIW-RUN (Figure 3b). Indeed, the EUC transport in the NOTIW-RUN is shown to increase again in June, reaching a second maximum in October, which is associated with a re-strengthening and shoaling of the EUC (Figure S3 in Supporting Information S1). However, as the EUC starts to decrease in spring and remains weak throughout the rest of the year, this second maximum mostly disappears in the TIW-RUN. The EUC re-intensification seems partly inhibited by the increased TIW activity starting in May/June in the TIW-RUN. Again, this could be linked to mechanisms of TIW-induced stabilization of the near surface flow (Figures 3c and 3d). This re-intensification of the EUC in the eastern Pacific is not observed in SODA v3.4.2 ocean reanalysis product (Figures S4 and S5 in Supporting Information S1), nor in in-situ observations (X. Yu and McPhaden (1999), their Figure 4). Note that due to the scarcity of EUC observations, we cannot apply the same diagnostics because it requires data over the entire latitudinal extent of the EUC. Thus, we can only hypothesize that this strong semi-annual cycle is not realistic.

Because the LR-RUN does not reproduce TIW variability accurately (see Section 3.1), it should be expected that the EUC seasonal cycle shape resembles that of the NOTIW-RUN. However, even though LR-RUN exhibits a weak EUC, its seasonal cycle matches that of the TIW-RUN, with no clear EUC re-intensification in October. The NONL-RUN, however, shows a very clear EUC semi-annual cycle, even more pronounced than in the NOTIW-RUN, even if the second peak in the transport, driven by the intensification of the core, is not accompanied by a shoaling like in NOTIW-RUN (Figure S3 in Supporting Information S1). This may indicate that a 1° horizontal resolution simulation resolves TIWs with sufficient strength to trigger this effect on the seasonal zonal equatorial circulation. This suggests the existence of a threshold in TIW activity beyond which the TIW-induced barotropic conversion is strong enough to stabilize the large-scale circulation, inhibiting the EUC re-intensification and preventing a potentially unrealistic semi-annual cycle.

4. Summary and Discussion

In this study, we assess the modulation of the eastern tropical Pacific seasonality by TIWs, using a regional ocean model. Following the methodology of Maillard et al. (2022), we compare a 1/12° regional eddy-rich simulation to one where TIWs are removed. We also consider a 1° simulation in which the coarse resolution prevents TIWs to be fully resolved, and a similar configuration where the nonlinear terms in the momentum equation are turned off to reduce the TIW activity even further.

Overall, our results highlight two types of seasonal changes of the eastern equatorial Pacific climate induced by TIWs:

- A direct (sub-monthly) effect on the upper ocean equatorial heat budget. This effect is driven by the TIW-induced NDH, which is itself modulated by the seasonal cycle. It leads to a meridional extension of the cold tongue, and to the weakening of the seasonal amplitude of the upper equatorial temperature and the meridional temperature gradient. This effect is not well captured by our 1° horizontal resolution simulation due to an underestimation of TIW activity.
- A rectified and delayed (one-to-two months) effect on the subsurface equatorial circulation that induces (a) a year-long weakening of the EUC of 0.15 m s^{-1} on average, most likely induced by the barotropic energy conversion that generates TIWs and leads to a stabilization of the upper ocean, along with (b) a change in the EUC seasonal phasing (i.e., an annualization of a potentially unrealistic semi-annual variability of the EUC in the absence of TIWs). This last effect does not seem proportional to TIW strength but rather triggered when TIW activity passes a certain threshold.

Note that these results hold when TIW-RUN is degraded to the similar coarse horizontal resolution as the LR-RUN (Figure S6 in Supporting Information S1).

The semi-annual variability of the eastern EUC has been noticed in several simulations of the eastern Pacific Ocean (e.g., Harrison et al. (2001) their Figure 1, Keenlyside and Kleeman (2002) their Figure 6b). To our knowledge, it has not been noticed in observations (X. Yu & McPhaden, 1999) that are nonetheless very sparse for the EUC, nor in the SODA v3.4.2 ocean reanalysis. Failing to simulate the eastern EUC seasonal cycle in low-resolution models could for instance cause an inaccurate shoaling of the EUC that may impact Kelvin waves through stratification changes, and influence ENSO initiation.

Using a simple conceptual 1-dimensional linear model, Boucharel and Jin (2020) have shown that the seasonal modulation of TIW activity (and thus of TIW induced NDH) could lead to a nonlinear rectification of the upper eastern Pacific temperatures (their Figure 6b). Based on their results, one would expect that TIWs could impact circulation via $-u'\nabla v'$ in the same way that TIWs impact temperature via NDH. It is not the case here, indicating that a new formulation of the theoretical framework of Boucharel and Jin (2020) is needed to better delineate the rectification effects of TIWs on both temperature and currents.

Finally, interestingly, the LR-RUN fails to reproduce the NDH effects of TIWs but manages to reproduce the seasonal cycle of the EUC. This indicates a need to develop scale-aware parameterizations in low-resolution models that do not properly resolve TIWs in order to reproduce more accurately the eastern Pacific Ocean.

Data Availability Statement

The CROCO model used in this study can be found here https://www.croco-ocean.org/. The data used to generate the figures can be found here https://doi.org/10.6084/m9.figshare.20597793.v1.

Acknowledgments
The NOAA Optimum Interpolation (OI) SST V2 data set can be found here https://psl.noaa.gov/data/gridded/data.noaa.oisst.v2.html. The GlobCurrent data set can be found here http://globcurrent.ifremer.fr/. This work was partly supported by the Thomas Jefferson Fund, a program of the FACE Foundation launched in

References

An, S.-I. (2008). Interannual variations of the tropical ocean instability wave and ENSO. *Journal of Climate*, *21*(15), 3680–3686. https://doi.org/10.1175/2008JCLI1701.1

An, S.-I., & Jin, F.-F. (2004). Nonlinearity and asymmetry of ENSO. *Journal of Climate*, *17*(12), 2399–2412. https://doi.org/10.1175/1520-0442(2004)017<2399:naaoe>2.0.co;2

Becker, J. J., Sandwell, D. T., Smith, W. H. F., Braud, J., Binder, B., Depner, J., et al. (2009). Global bathymetry and elevation data at 30 arc seconds resolution: SRTM30_PLUS. *Marine Geodesy*, *32*(4), 355–371. https://doi.org/10.1080/01490410903297766

Boucharel, J., & Jin, F.-F. (2020). A simple theory for the modulation of tropical instability waves by ENSO and the annual cycle. *Tellus A: Dynamic Meteorology and Oceanography*, *72*(1), 1–14. https://doi.org/10.1080/16000870.2019.1700087

collaboration with the French Embassy in the U.S. LM and JB are funded through the French Agence Nationale de la Recherche project Make Our Planet Great Again MOPGA "Trocodyn" (ANR-17-MPGA-0018) and the Région Occitanie. LR is funded through the French ANR EUREC4 project, the CNES TOSCA I-CASCADE project and the CARAMBA project. F.-F.J. is funded through the U.S. National Science Fundation Grant AG-S-1813611 and the U.S. Department of Energy Grant D-E-SC0005110. In addition, MFS was supported by NSF grant AGS-2141728 and NOAA's Climate Program Office's Modeling, Analysis, Predictions, and Projections (MAPP) program grant NA20OAR4310445. We thank the CALMIP and GENCI centers for providing access to the supercomputers Olympe and Irene (project 13051). We thank two anonymous reviewers for their constructive comments. This is SOEST publication 11598 and IPRC contribution 1585.

Carton, J. A., Chepurin, G. A., & Chen, L. (2018). SODA3: A new ocean climate reanalysis. *Journal of Climate*, *31*(17), 6967–6983. https://doi.org/10.1175/JCLI-D-18-0149.1

Chelton, D. B., Esbensen, S. K., Schlax, M. G., Thum, N., Freilich, M. H., Wentz, F. J., et al. (2001). Observations of coupling between surface wind stress and sea surface temperature in the eastern tropical Pacific. *Journal of Climate*, *14*(7), 1479–1498. https://doi.org/10.1175/1520-0442(2001)014<1479:oocbsw>2.0.co;2

Contreras, R. F. (2002). Long-term observations of tropical instability waves. *Journal of Physical Oceanography*, *32*(9), 8–2722. https://doi.org/10.1175/1520-0485-32.9.2715

Cox, M. (1980). Generation and propagation of 30-day waves in a numerical model of the Pacific. *Journal of Physical Oceanography, American Meteorological Society*, *10*(8), 1168–1186. https://doi.org/10.1175/1520-0485(1980)010<1168:gapodw>2.0.co;2

Debreu, L., Marchesiello, P., Penven, P., & Cambon, G. (2012). Two-way nesting in split-explicit ocean models: Algorithms, implementation and validation. *Ocean Modelling*, *49–50*, 1–21. https://doi.org/10.1016/j.ocemod.2012.03.003

Düing, W., Hisard, P., Katz, E., Meincke, J., Miller, L., Moroshkin, K. V., et al. (1975). Meanders and long waves in the equatorial Atlantic. *Nature*, *257*(5524), 280–284. https://doi.org/10.1038/257280a0

Eddebbar, Y. A., Subramanian, A. C., Whitt, D. B., Long, M. C., Verdy, A., Mazloff, M. R., & Merrifield, M. A. (2021). Seasonal modulation of dissolved oxygen in the equatorial Pacific by tropical instability vortices. *Journal of Geophysical Research: Oceans*, *126*(11), e2021JC017567. https://doi.org/10.1029/2021JC017567

Escobar-Franco, M. G., Boucharel, J., & Dewitte, B. (2022). On the relationship between tropical instability waves and intraseasonal equatorial kelvin waves in the Pacific from satellite observations (1993–2018). *Frontiers in Marine Science*, *9*, 788908. https://doi.org/10.3389/fmars.2022.788908

Eyring, V., Bony, S., Meehl, G. A., Senior, C. A., Stevens, B., Stouffer, R. J., & Taylor, K. E. (2016). Overview of the Coupled Model Intercomparison Project Phase 6 (CMIP6) experimental design and organization. *Geoscientific Model Development*, *9*(5), 1937–1958. https://doi.org/10.5194/gmd-9-1937-2016

Fairall, C. W., Bradley, E. F., Hare, J. E., Grachev, A. A., & Edson, J. B. (2003). Bulk Parameterization of air–sea fluxes: Updates and verification for the COARE algorithm. *Journal of Climate*, *16*(4), 571–591. https://doi.org/10.1175/1520-0442(2003)016<0571:bpoasf>2.0.co;2

Graham, T. (2014). The importance of eddy permitting model resolution for simulation of the heat budget of tropical instability waves. *Ocean Modelling*, *79*, 21–32. https://doi.org/10.1016/j.ocemod.2014.04.005

Gruber, N., Lachkar, Z., Frenzel, H., Marchesiello, P., Münnich, M., McWilliams, J. C., et al. (2011). Eddy-induced reduction of biological production in eastern boundary upwelling systems. *Nature Geoscience*, *4*(11), 787–792. https://doi.org/10.1038/ngeo1273

Harrison, D. E., Romea, R. D., & Vecchi, G. A. (2001). Central equatorial Pacific zonal currents. II: The seasonal cycle and the boreal spring surface eastward surge. *Journal of Marine Research*, *59*(6), 921–948. https://doi.org/10.1357/00222400160497715

Holmes, R. M., & Thomas, L. N. (2015). The modulation of equatorial turbulence by tropical instability waves in a regional ocean model. *Journal of Physical Oceanography*, *45*(4), 1155–1173. https://doi.org/10.1175/JPO-D-14-0209.1

Holmes, R. M., & Thomas, L. N. (2016). Modulation of tropical instability wave intensity by equatorial kelvin waves. *Journal of Physical Oceanography*, *46*(9), 2623–2643. https://doi.org/10.1175/JPO-D-16-0064.1

Im, S.-H., An, S.-I., Lengaigne, M., & Noh, Y. (2012). Seasonality of tropical instability waves and its feedback to the seasonal cycle in the tropical eastern Pacific. *The Scientific World Journal*, *2012*, 1–11. https://doi.org/10.1100/2012/612048

Inoue, R., Lien, R.-C., & Moum, J. N. (2012). Modulation of equatorial turbulence by a tropical instability wave. *Journal of Geophysical Research*, *117*(C10), L24607. https://doi.org/10.1029/2011JC007767

Keenlyside, N., & Kleeman, R. (2002). Annual cycle of equatorial zonal currents in the Pacific. *Journal of Geophysical Research*, *107*(C8), 3093. https://doi.org/10.1029/2000JC000711

lanKuo, H. (1949). Dynamic instability of two-dimensional nondivergent flow in a barotropic atmosphere. *Journal of the Atmospheric Sciences*, *6*(2), 105–122. https://doi.org/10.1175/1520-0469(1949)006<0105:diotdn>2.0.co;2

Large, W. G., McWilliams, J. C., & Doney, S. C. (1994). Oceanic vertical mixing: A review and a model with a nonlocal boundary layer parameterization. *Reviews of Geophysics*, *32*(4), 363. https://doi.org/10.1029/94RG01872

Lee, T., Lagerloef, G., Gierach, M. M., Kao, H.-Y., Yueh, S., & Dohan, K. (2012). Aquarius reveals salinity structure of tropical instability waves. *Geophysical Research Letters*, *39*(12), L12610. https://doi.org/10.1029/2012GL052232

Legeckis, R. (1977). Long waves in the eastern equatorial Pacific ocean: A view from a geostationary satellite. *Science*, *197*(4309), 1179–1181. https://doi.org/10.1126/science.197.4309.1179

Lien, R.-C., D'Asaro, E. A., & Menkes, C. E. (2008). Modulation of equatorial turbulence by tropical instability waves. *Geophysical Research Letters*, *35*(24), L24607. https://doi.org/10.1029/2008GL035860

Lyman, J. M., Johnson, G. C., & Kessler, W. S. (2007). Distinct 17- and 33-day tropical instability waves in subsurface observations. *Journal of Physical Oceanography*, *37*(4), 855–872. https://doi.org/10.1175/JPO3023.1

Maillard, L., Boucharel, J., & Renault, L. (2022). Direct and rectified effects of tropical instability waves on the eastern tropical Pacific mean state in a regional ocean model. *Journal of Physical Oceanography*, *52*(8), 1817–1834. https://doi.org/10.1175/JPO-D-21-0300.1

Masina, S., Philander, S. G. H., & Bush, A. B. G. (1999). An analysis of tropical instability waves in a numerical model of the Pacific ocean: 2. Generation and energetics of the waves. *Journal of Geophysical Research*, *104*(C12), 29637–29661. https://doi.org/10.1029/1999JC900226

Menkes, C. E. R., Vialard, J. G., Kennan, S. C., Boulanger, J.-P., & Madec, G. V. (2006). A modeling study of the impact of tropical instability waves on the heat budget of the eastern equatorial Pacific. *Journal of Physical Oceanography*, *36*(5), 847–865. https://doi.org/10.1175/JPO2904.1

Miller, L., Watts, D. R., & Wimbush, M. (1985). Oscillations of dynamic topography in the eastern equatorial Pacific. *Journal of Physical Oceanography*, *15*(12), 1759–1770. https://doi.org/10.1175/1520-0485(1985)015<1759:oodtit>2.0.co;2

Moum, J. N., Lien, R.-C., Perlin, A., Nash, J. D., Gregg, M. C., & Wiles, P. J. (2009). Sea surface cooling at the Equator by subsurface mixing in tropical instability waves. *Nature Geoscience*, *2*(11), 761–765. https://doi.org/10.1038/ngeo657

Philander, S. G. H. (1976). Instabilities of zonal equatorial currents. *Journal of Geophysical Research*, *11*(C7), 3679. https://doi.org/10.1029/jc083ic07p03679

Philander, S. G. H. (1978). Instabilities of zonal equatorial currents, 2. *Journal of Geophysical Research*, *83*(C7), 3679. https://doi.org/10.1029/JC083iC07p03679

Qiao, L., & Weisberg, R. H. (1995). Tropical instability wave kinematics: Observations from the tropical instability wave experiment. *Journal of Geophysical Research*, *100*(C5), 8677. https://doi.org/10.1029/95JC00305

Renault, L., Masson, S., Arsouze, T., Madec, G., & McWilliams, J. C. (2020). Recipes for how to force oceanic model dynamics. *Journal of Advances in Modeling Earth Systems*, *12*(2), e2019MS001715. https://doi.org/10.1029/2019MS001715

Renault, L., Molemaker, M. J., Mcwilliams, J. C., Shchepetkin, A. F., Lemarié, F., Chelton, D., et al. (2016). Modulation of wind work by oceanic current interaction with the atmosphere. *Journal of Physical Oceanography*, *46*(6), 20–1704. https://doi.org/10.1175/jpo-d-15-0232.1

Reynolds, R. W., Smith, T. M., Liu, C., Chelton, D. B., Casey, K. S., & Schlax, M. G. (2007). Daily high-resolution-blended analyses for sea surface temperature. *Journal of Climate*, *20*(22), 5473–5496. https://doi.org/10.1175/2007JCLI1824.1

Rio, M.-H., Mulet, S., & Picot, N. (2014). Beyond GOCE for the ocean circulation estimate: Synergetic use of altimetry, gravimetry, and in situ data provides new insight into geostrophic and Ekman currents. *Geophysical Research Letters*, *41*(24), 8918–8925. https://doi.org/10.1002/2014GL061773

Saha, S., Moorthi, S., Pan, H.-L., Wu, X., Wang, J., Nadiga, S., et al. (2010). *NCEP climate forecast system reanalysis (CFSR) selected hourly time-series products, January 1979 to December 2010*. Research Data Archive at the National Center for Atmospheric Research, Computational and Information Systems Laboratory.

Saha, S., Moorthi, S., Wu, X., Wang, J., Nadiga, S., Tripp, P., et al. (2011). *NCEP climate forecast system version 2 (CFSv2) selected hourly time-series products*. Research Data Archive at the National Center for Atmospheric Research, Computational and Information Systems Laboratory. https://doi.org/10.5065/D6N877VB

Shchepetkin, A. F. (2015). An adaptive, courant-number-dependent implicit scheme for vertical advection in oceanic modeling. *Ocean Modelling*, *91*, 38–69. https://doi.org/10.1016/j.ocemod.2015.03.006

Shchepetkin, A. F., & McWilliams, J. C. (2005). The regional oceanic modeling system (ROMS): A split-explicit, free-surface, topography-following-coordinate oceanic model. *Ocean Modelling*, *58*(4), 347–404. https://doi.org/10.1016/j.ocemod.2004.08.002

Shchepetkin, A. F., & McWilliams, J. C. (2009). Correction and commentary for "Ocean forecasting in terrain-following coordinates: Formulation and skill assessment of the regional ocean modeling system" by Haidvogel et al. *Journal of Computational Physics*, *228*(24), 8985–9000. https://doi.org/10.1016/j.jcp.2009.09.002

Stuecker, M. F., Timmermann, A., Jin, F.-F., McGregor, S., & Ren, H.-L. (2013). A combination mode of the annual cycle and the El Niño/Southern Oscillation. *Nature Geoscience*, *6*(7), 540–544. https://doi.org/10.1038/ngeo1826

Takahashi, T., Sutherland, S. C., Wanninkhof, R., Sweeney, C., Feely, R. A., Chipman, D. W., et al. (2009). Climatological mean and decadal change in surface ocean pCO_2, and net sea–air CO_2 flux over the global oceans. *Deep Sea Research Part II: Topical Studies in Oceanography*, *56*(8), 554–577. (Surface Ocean CO2 Variability and Vulnerabilities). https://doi.org/10.1016/j.dsr2.2008.12.009

Vialard, J. R. M., Menkes, C., Boulanger, J.-P., Delecluse, P., Guilyardi, E., Mcphaden, M. J., & Madec, G. (2001). A model study of oceanic mechanisms affecting equatorial Pacific sea surface temperature during the 1997–98 El Niño. *Journal of Physical Oceanography*, *31*(7), 27–1675. https://doi.org/10.1175/1520-0485(2001)031<1649:amsoom>2.0.co;2

Von Schuckmann, K., Brandt, P., & Eden, C. (2008). Generation of tropical instability waves in the Atlantic Ocean. *Journal of Geophysical Research*, *113*(C8), C08034. https://doi.org/10.1029/2007JC004712

Wang, M., Du, Y., Qiu, B., Xie, S.-P., & Feng, M. (2019). Dynamics on seasonal variability of EKE associated with TIWs in the eastern equatorial Pacific Ocean. *Journal of Physical Oceanography*, *49*(6), 1503–1519. https://doi.org/10.1175/JPO-D-18-0163.1

Wang, M., Xie, S.-P., Shen, S. S. P., & Du, Y. (2020). Rossby and Yanai modes of tropical instability waves in the equatorial Pacific ocean and a diagnostic model for surface currents. *Journal of Physical Oceanography*, *50*(10), 3009–3024. https://doi.org/10.1175/JPO-D-20-0063.1

Wang, W., & McPhaden, M. J. (2000). The surface-layer heat balance in the equatorial Pacific Ocean. Part II: Interannual variability. *Journal of Physical Oceanography*, *30*(11), 2989–3008. https://doi.org/10.1175/1520-0485(2001)031<2989:tslhbi>2.0.co;2

Wang, W., & McPhaden, M. J. (2001). Surface layer temperature balance in the equatorial Pacific during the 1997–98 El Niño and 1998–99 La Niña. *Journal of Climate*, *14*(16), 3393–3407. https://doi.org/10.1175/1520-0442(2001)014<3393:sltbit>2.0.co;2

Xie, S.-P., Ishiwatari, M., Hashizume, H., & Takeuchi, K. (1998). Coupled ocean-atmospheric waves on the equatorial front. *Geophysical Research Letters*, *25*(20), 3863–3866. https://doi.org/10.1029/1998GL900014

Xue, A., Jin, F.-F., Zhang, W., & Boucharel, J. (2022). Quantifying ENSO-tropical instability waves (TIWs) interaction by nonlinear Eddy thermal diffusivity. *Submitted to Journal of Geophysical Research: Ocean*.

Xue, A., Jin, F.-F., Zhang, W., Boucharel, J., Zhao, S., & Yuan, X. (2020). Delineating the seasonally modulated nonlinear feedback onto ENSO from tropical instability waves. *Geophysical Research Letters*, *47*(7). https://doi.org/10.1029/2019GL085863

Xue, A., Zhang, W., Boucharel, J., & Jin, F.-F. (2021). Anomalous tropical instability wave activity hindered the development of the 2016/17 La Niña. *Journal of Climate*, *34*(13), 5583–5600. https://doi.org/10.1175/JCLI-D-20-0399.1

Yu, X., & McPhaden, M. J. (1999). Seasonal variability in the equatorial Pacific. *Journal of Physical Oceanography*, *29*(5), 925–947. https://doi.org/10.1175/1520-0485(1999)029<0925:svitep>2.0.co;2

Yu, Z., McCreary, J. P., & Proehl, J. A. (1995). Meridional asymmetry and energetics of tropical instability waves. *Journal of Physical Oceanography*, *25*(12), 2997–3007. https://doi.org/10.1175/1520-0485(1995)025<2997:maaeot>2.0.co;2